

# Magnetic Resonance Imaging using Optimized 2D NUFFTs

Amedeo Capozzoli, Claudio Curcio, and Angelo Liseno

Università di Napoli Federico II  
 Dipartimento di Ingegneria Elettrica e delle Tecnologie dell'Informazione  
 via Claudio 21, I 80125 Napoli (Italy)

**Abstract** — We propose optimized 2D Non-Uniform FFT (NUFFT) algorithms and apply them to Magnetic Resonance Imaging under radial acquisitions.

**Index Terms** — Filtered Backprojection, MRI, NUFFT.

## I. INTRODUCTION

In MRI, much effort has been devoted to acquisition methods using non-Cartesian grids [1] such as radial scannings for fast data acquisition. Radial scans [2] are, for example, less prone to residual motion and changes of the imaging plane during interactive scanning making them attractive tools for image-guided interventions [3].

Due to the non-regular grid, the use of standard FFTs to process non-Cartesian data breaks down under radial scans so that MRI imaging requires more involved data processing to properly balance accuracy and computational burden in this case. Fortunately, Non-Uniform FFT (NUFFT) provide a convenient trade-off between accuracy and complexity [1, 4, 5, 6].

Recently, an optimized NUFFT approach, based on a new and general perspective, has been presented in [6]. The choice of the window function has been optimized to obtain more accurate results than those available in the literature. The computational costs and the memory requirements of the proposed schemes have been theoretically analyzed and their very convenient performance assessed, theoretically and numerically, by comparisons with a number of relevant and popular approaches. The proposed method has proved to be more accurate than all the confronted schemes without burdening the computational and memory requirements.

The purpose of this paper is presenting an improvement over the approach in [6] in which we introduce the “optimized” NUFFTs, also in their 2D formulations, for radial MRI processing.

## II. NUFFT-BASED MRI RECONSTRUCTION

The signal  $r$  acquired by the coils of an MRI system is related to the spin density  $\rho$  in a 2D case considered for the sake of convenience, by:

$$r(k_x(t), k_y(t)) = \iint_{\mathcal{O}} S(x, y)\rho(x, y)e^{-j2\pi[k_x(t)x+k_y(t)y]}d\mathcal{O}, \quad (1)$$

where  $S$  is the receiving coil sensitivity map,  $\underline{k}(t) = (k_x(t), k_y(t))$  denotes the  $k$ -space trajectory and  $\mathcal{O}$  is the Region of Interest (ROI).

Using a pixel-based approximation for  $\rho$  and sampling the signal  $r$  at the time instants  $t_n$ , eq. (1) is regarded as a system of linear equations:

$$\underline{A}\underline{\rho} = \underline{r}, \quad (2)$$

where  $r$  is the data vector whose generic element is  $r_n = r(k_x(t_n), k_y(t_n))$  and  $\underline{\rho}$  is the unknowns vector containing the unknown pixel values  $\rho_s$ .

The generic element  $A_{ns}$  of  $\underline{A}$  is provided by:

$$A_{ns} = S(x_s, y_s)e^{-j2\pi[k_x(t_n)x_s+k_y(t_n)y_s]}\Delta x\Delta y, \quad (3)$$

with  $\Delta x\Delta y$  the pixel size.

A pseudosolution to (2) is typically searched for by solving the associated Euler equation:

$$\underline{A}^+\underline{A}\underline{\rho} = \underline{b}, \quad (4)$$

where  $\underline{b} = \underline{A}^+\underline{r}$  and  $\underline{A}^+$  is the adjoint matrix of  $\underline{A}$  whose generic element  $A_{sn}^+$  is  $A_{ns}^*$ , where  $*$  denotes the complex conjugation. Eq. (4) is then solved by using iterative techniques minimizing the error functional:

$$\Phi(\underline{\rho}) = \|\underline{A}^+\underline{A}\underline{\rho} - \underline{A}^+\underline{r}\|^2. \quad (5)$$

The matrix-vector multiplications involving matrices  $\underline{A}$  and  $\underline{A}^+$  can be computed by 2D NUFFTs of Non-Equispaced Results (NER) and Non-Equispaced Data (NED), respectively. We recall 1D NER and NED Non-Uniform DFTs, for simplicity, but the results will regard the 2D case.

The 1D NER NUDFT of uniform samples  $\{z_k\}_{k=-N/2}^{N/2-1}$ , evaluated at non-equispaced grid points  $\tilde{x}_l \in \left[-\frac{N}{2}, \frac{N}{2}\right]$ , is defined as:

$$\tilde{z}_l = \sum_{k=-N/2}^{N/2-1} z_k e^{-j2\pi\tilde{x}_l \frac{k}{N}}, \quad l = 1, \dots, M. \quad (6)$$

The 1D NED NUFT of samples  $\{z_l\}_{l=1}^M$ , located at non-equispaced points  $\{\tilde{x}_l\}_{l=1}^M$  and evaluated on an equispaced grid, is defined as:

$$\hat{z}_l = \sum_{l=1}^M z_l e^{-j2\pi\tilde{x}_l \frac{k}{N}}, \quad k = -\frac{N}{2}, \dots, \frac{N}{2} - 1. \quad (7)$$

### III. NUMERICAL RESULTS

We show the performance of the optimized NER- and NED-NUFT algorithms for 2D.

The NER accuracy is assessed in the case of  $12 \times 12$ , complex, non-uniformly and randomly distributed sampling points generated in the  $[-6,6]m^{-1} \times [-6,6]m^{-1}$  spectral region. Real and imaginary parts uniformly distributed in  $[-0.5,0.5]$  have been assumed. Tables 1 and 2 illustrate the accuracy in terms of Root Mean Square (RMS) errors and maximum errors as compared to the corresponding NER-NUFT for single and double precision arithmetics, respectively. In both the cases, the performance is compared to the scheme in [4]. The optimized NUFT is compared also with that in [1] which is available for single precision only. As it can be seen, our approach outperforms the compared ones.

The NED performance is illustrated by showing the result of the computation of  $\underline{\underline{A}}^\dagger \underline{\underline{A}} \underline{\underline{\rho}}$  which amounts at the so-called Filtered Backprojection (FPB) algorithm for radial MRI acquisitions. Fig. 1 illustrates the radial spectral sample locations, while Fig. 2 depicts the reconstruction of the Shepp-Logan phantom. Accuracies similar to those in Table 1 are achieved.

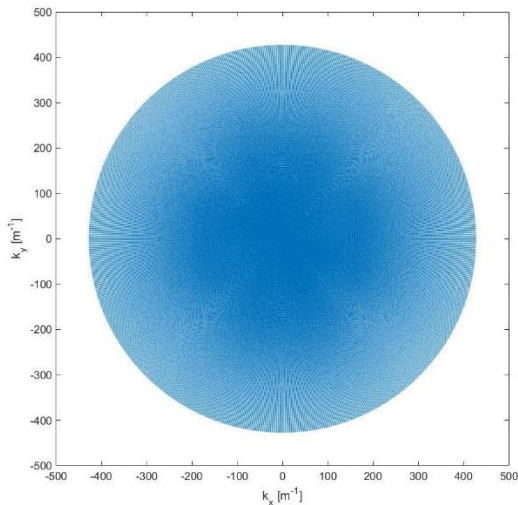


Fig. 1. Radial sample locations.

Table 1: RMS and maximum errors: Single precision

	Type-2 NUFT Algorithm		
	<i>KB</i>	<i>Optimized</i>	<i>Fessler</i>
<b>RMS</b>	$6.23 \cdot 10^{-4}$	$1.11 \cdot 10^{-4}$	$122 \cdot 10^{-4}$
<b>MAX</b>	$6.93 \cdot 10^{-5}$	$1.12 \cdot 10^{-5}$	$140 \cdot 10^{-5}$

Table 1: RMS and maximum errors: Double precision

	Type-2 NUFT Algorithm	
	<i>KB</i>	<i>Optimized</i>
<b>RMS</b>	$5.40 \cdot 10^{-10}$	$8.87 \cdot 10^{-11}$
<b>MAX</b>	$7.92 \cdot 10^{-10}$	$1.73 \cdot 10^{-10}$

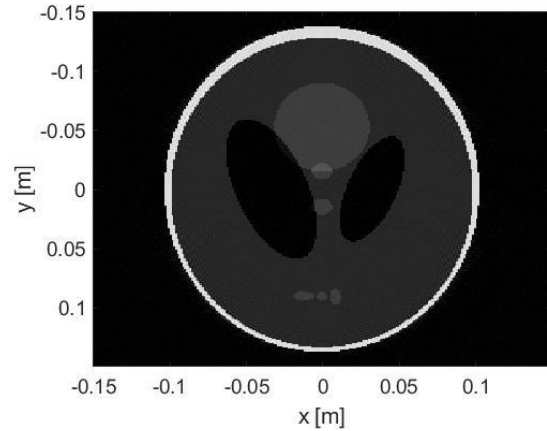


Fig. 2. Phantom reconstruction.

### REFERENCES

- [1] J. A. Fessler, "On NUFT-based gridding for non-Cartesian MRI," *J. Magn. Res.*, vol. 188, no. 2, pp. 191-195, Oct. 2007.
- [2] S. Konstandin, A. M. Nagel, P. M. Heiler, and L. R. Schad, "Two-dimensional radial acquisition technique with density adaption in sodium MRI," *Mag. Res. Med.*, vol. 65, no. 4, pp. 1091-1097, Apr. 2011.
- [3] M. Uecker, S. Zhang, D. Voit, K.-D. Merboldt, and J. Frahm, "Real-time MRI: recent advances using radial FLASH," *Imaging in Medicine*, vol. 4, no. 4, pp. 461-476, 2012.
- [4] K. Fourmont, "Non-Equispaced fast fourier transforms with applications to tomography," *J. Fourier Anal. Appl.*, vol. 9, no. 5, pp. 431-450, Sept. 2003.
- [5] A. Capozzoli, C. Curcio, A. Di Vico, and A. Liseno, "NUFT- & GPU-based fast imaging of vegetation," *IEICE Trans. Commun.*, vol. E94-B, no. 7, pp. 2092-2103, July 2011.
- [6] A. Capozzoli, C. Curcio, and A. Liseno, "Optimized non-uniform FFTs (NUFTs) and their application to array factor computation," *IEEE Trans. Antennas Prop.*, vol. 67, no. 6, pp. 3924-3938, June 2019.